Available online at www.sciencedirect.com

SciVerse ScienceDirect

journal homepage: www.elsevier.com/locate/watres

Morphological and physicochemical characteristics of iron corrosion scales formed under different water source histories in a drinking water distribution system

Fan Yang [a,c], Baoyou Shi [a,*], Junnong Gu [b], Dongsheng Wang [a], Min Yang [a]

[a] State Key Laboratory of Environmental Aquatic Chemistry, Research Center for Eco-Environmental Sciences, Chinese Academy of Sciences, 18 Shuangqing Road, P.O. Box 2871, Beijing 100085, China

[b] Center for Water Quality Monitoring, Beijing Waterworks Group, Beijing 100192, China

[c] Graduate School, Chinese Academy of Sciences, Beijing 100039, China

ARTICLE INFO

Article history:
Received 7 May 2012
Received in revised form
12 July 2012
Accepted 15 July 2012
Available online 25 July 2012

Keywords:
Corrosion scale
Morphology
Magnetite/goethite ratio
Water source history
Drinking water distribution system

ABSTRACT

The corrosion scales on iron pipes could have great impact on the water quality in drinking water distribution systems (DWDS). Unstable and less protective corrosion scale is one of the main factors causing "discolored water" issues when quality of water entering into distribution system changed significantly. The morphological and physicochemical characteristics of corrosion scales formed under different source water histories in duration of about two decades were systematically investigated in this work. Thick corrosion scales or densely distributed corrosion tubercles were mostly found in pipes transporting surface water, but thin corrosion scales and hollow tubercles were mostly discovered in pipes transporting groundwater. Magnetite and goethite were main constituents of iron corrosion products, but the mass ratio of magnetite/goethite (M/G) was significantly different depending on the corrosion scale structure and water source conditions. Thick corrosion scales and hard shell of tubercles had much higher M/G ratio (>1.0), while the thin corrosion scales had no magnetite detected or with much lower M/G ratio. The M/G ratio could be used to identify the characteristics and evaluate the performances of corrosion scales formed under different water conditions. Compared with the pipes transporting ground water, the pipes transporting surface water were more seriously corroded and could be in a relatively more active corrosion status all the time, which was implicated by relatively higher siderite, green rust and total iron contents in their corrosion scales. Higher content of unstable ferric components such as γ-FeOOH, β-FeOOH and amorphous iron oxide existed in corrosion scales of pipes receiving groundwater which was less corroded. Corrosion scales on groundwater pipes with low magnetite content had higher surface area and thus possibly higher sorption capacity. The primary trace inorganic elements in corrosion products were Br and heavy metals. Corrosion products obtained from pipes transporting groundwater had higher levels of Br, Ti, Ba, Cu, Sr, V, Cr, La, Pb and As.

* *Corresponding author*. Tel./fax: +86 10 62849138.
E-mail address: byshi@rcees.ac.cn (B. Shi).

0043-1354/$ – see front matter © 2012 Elsevier Ltd. All rights reserved.
http://dx.doi.org/10.1016/j.watres.2012.07.031

1. Introduction

Internal corrosion of metallic pipes is ubiquitous in drinking water distribution systems (DWDS). Corrosion scales formed by the accumulation of corrosion products could serve as the breeding ground for microbes and sinks for heavy metals or other contaminants (e.g., arsenic, vanadium, lead) (Peng et al., 2010, 2012; Sarin et al., 2001; Tuovinen and Hsu, 1982; Tuovinen et al., 1980). Inorganic contaminants presented only at trace levels in finished waters tend to accumulate in DWDS corrosion solids where their concentration can exceed those in solution by several orders of magnitude (Peng et al., 2010, 2012). Disturbance of corrosion scales or biofilms caused by water quality changes might result in discolored water episodes, microbial film loosening and sorbed contaminants release. Deterioration of water quality in DWDS would lead to consumer complaints and potentially threaten human health.

The formation process and physicochemical characteristics of corrosion scales in drinking water pipes depend on the metallic materials of pipes, the contacted water quality, and possibly the hydraulic conditions, etc. The water quality parameters relevant to corrosion process include pH, alkalinity, buffer intensity, dissolved oxygen (DO), natural organic matter (NOM), microorganisms, temperature, inhibitor if applied, and so on (Gerke et al., 2008; McNeill and Edwards, 2001; Ray et al., 2010; Sarin et al., 2001, 2004a,b). Under some circumstances, variations in water quality could disturb the solid–liquid equilibrium between corrosion scale and water phase, and consequently adversely affect water quality in distribution systems.

There have been several reports about serious red water cases owing to source water switch, such as in South California, Tucson Arizona and Tampa Florida in the United States (Reiber et al., 1997; Brodeur et al., 2006; Tang et al., 2006). Red water issue had occurred in some areas in a northern city of China, soon after 80% of the local source water was replaced by long-distance introduced source water from a neighboring province in October, 2008. It was interesting to find that heavy red water occurred only in areas historically supplying local groundwater, and the areas without red water were historically supplied with local surface waters. The Tucson and Florida red water cases were also trigged by the source water switch from ground waters to surface waters. These facts indicated that the corrosion scales might have distinct characteristics depending on their historically contacted water quality and different corrosion scales might have different adaptability to source water switch.

Water supply industries worldwide are investing large amount of capitals in repairing and replacing distribution pipes as well as developing strategies to deal with “discolored water” issues (AWWA, 1996; AWWA, 1999). Cast iron and steel pipes were still holding a large proportion in drinking water distribution systems in many countries, for example, 56.6% in USA, 67.2% in Italy (Świetlik et al., 2012) and 75.5% in China (Wang, 2007). Corrosion of iron pipes can lead to the damage of distribution system infrastructure, loss of water transportation capacity and deterioration of water quality. Particularly, the common red water issues are closely correlated with the release of iron corrosion products. To better understand the mechanisms triggering the emergence of red water and develop suitable plans for source water switch, it is very imperative to investigate the physicochemical characteristics and performances of corrosion scales formed under different water quality conditions.

Numerous studies have been dedicated to understand the iron corrosion scale properties (Tuovinen et al., 1980; Benjamin et al., 1996; Lin et al., 2001; Sarin et al., 2001, 2004a,b; Gerke et al., 2008; Peng et al., 2010, 2012; Świetlik et al., 2012); however, to our knowledge, no research work had focused on the characterization of corrosion scales with different source water histories. Several researchers have described the detailed morphologies of some iron corrosion scales and the classical multilayered structure of tubercles was demonstrated (Sarin et al., 2004b; Gerke et al., 2008). According to the most popular model, corrosion scales contain a four-layered structure: a surface layer, a hard shell-like layer and a porous core layer over a corroding floor (Sarin et al., 2001, 2004b). Gerke et al. (2008) gave a detailed description of vein-like feature in core region and metal concentration in different layers for five tubercles from three 90-year-old cast iron pipes. Peng et al. (2010) collected 46 pipe samples from 20 drinking water utilities with different water source for detailed elemental analysis, but the morphology, microstructure and chemical composition characteristics owing to different water source had not been elucidated. Besides, the corrosion scale samples for X-ray diffraction analysis, one of the most commonly used techniques, were usually dried in air and it was observed that the crystalline composition of corrosion scales could change quickly under atmosphere (Świetlik et al., 2012).

The aim of this work is to provide a systematic investigation of physicochemical and micro-structural characteristics of corrosion scales with different source water histories in DWDS. The corrosion scale samples were carefully protected against oxygen, pretreated in inert atmosphere, vacuum-freeze-dried and characterized as soon as possible. Statistical method was used to compare scale property differences. Evolutionary polynomial regression was applied to reveal the relationship between surface area of scale samples and their mineral composition, and the sensitivity of the explanatory variables was also discussed. The findings of this work could help to understand the mechanisms of red water cases after source water switch and develop technological strategies to avoid red water occurrence in DWDSs.

2. Materials and methods

2.1. *Sample collection*

Old unlined cast iron pipe sections (approximately 20–25 years old) were excavated from 12 different DWDS sites in the city of Beijing. These sites were supplied with finished waters from different water sources. Water source type, main finished water quality parameters and treatment processes of corresponding water treatment plants (WTPs) are summarized in Table 1. The identification (ID) of each pipe section

Table 1 – Water source, finished water quality, and main water treatment units.

Treatment plant	SWTP1	SWTP2	SWTP3	GWTP1	GWTP2	GWTP3
Water source	Surface water 1	Surface water 2	Surface water 3	Groundwater 1	Groundwater 2	Groundwater 3
pH	7.74	7.84	7.88	7.70	7.46	7.60
Temperature (°C)	4–25 (12.9)[a]	3–26 (13.8)	1–29 (15.6)	4–25 (13.8)	6–19 (14.4)	11–18 (15.0)
Alkalinity (mg/L $CaCO_3$)	141.0	155.0	139.0	165.5	241.0	198.6
Cl_2 (mg/L)	0.73	0.68	0.70	0.62	0.61	0.63
Al (mg/L)	<0.018	<0.018	<0.985	<0.039	<0.016	<0.005
Fe (mg/L)	<0.05	<0.09	<0.06	<0.05	<0.06	<0.05
Mn (mg/L)	<0.002	<0.002	<0.001	<0.002	<0.002	<0.001
Cu (mg/L)	<0.001	<0.002	<0.001	<0.001	<0.001	<0.001
Zn (mg/L)	<0.05	<0.07	<0.05	<0.05	<0.05	<0.05
K (mg/L)	2.8	2.4	3.2	2.2	2.8	1.90
Ca (mg/L $CaCO_3$)	119	116	117	133	217	133
Na (mg/L)	13.5	12.8	17.6	12.9	39.4	15.0
Mg (mg/L $CaCO_3$)	70.5	82.5	76.0	72.5	136.5	83.0
Chloride (mg/L)	21.0	15.7	19.6	18.7	57.7	14.3
Sulfate (mg/L)	52.1	50.7	74.1	38.0	99.1	22.3
Larson ratio	0.59	0.48	0.76	0.40	0.77	0.22
Water treatment train	Coagulation, sedimentation, filtration, activated carbon adsorption, disinfection	Coagulation, sedimentation, filtration, ozonation-biologically activated carbon, disinfection	Coagulation, sedimentation, filtration, activated carbon adsorption, disinfection	Disinfection	Disinfection	Disinfection

a Temperature range and average value.

and the corresponding WTP, water source and pipe diameter are presented in Table 2. Four of the 12 pipe sections, PipeD, PipeE, PipeF and PipeG were transporting blended ground and surface waters, since they were excavated from the boundary of ground and surface water service areas.

Inner view pictures of pipe section samples were taken immediately after excavated. Typical corrosion scale samples with different appearances were collected from freshly obtained pipe sections. Some scale samples were saved for SEM–EDX (Scanning Electron Microscope–Energy Dispersive X-ray spectroscopy) analysis, and some were pretreated for X-ray diffraction (XRD), total organic carbon (TOC), X-ray Fluorescence (XRF), Raman spectroscopy, surface area and pore analysis, free and amorphous iron analysis, as soon as possible. The pretreatment procedures were as follows: samples were pulverized in an anaerobic glove box and passed through a 150 μm mesh sieve, then vacuum-freeze-dried. Pretreatment under aerobic and anaerobic conditions were also compared to investigate their possible effects on the composition of corrosion products.

Table 2 – Pipe section ID, water treatment plant, water source and pipe diameter.[a]

Pipe section ID	Treatment plant	Water source	Pipe diameter (mm)
Pipe-SW1	SWTP1	SW1	100
Pipe-SW2	SWTP2	SW2	100
Pipe-SW3	SWTP3	SW3	100
PipeA-GW1	GWTP1	GW1	100
PipeB-GW1	GWTP1	GW1	100
PipeA-GW3	GWTP3	GW3	600
PipeB-GW3	GWTP3	GW3	100
PipeC-GW3	GWTP3	GW3	100
PipeD-SW1/GW2	SWTP1, GWTP2	SW1, GW2	70
PipeE-SW1/GW1	SWTP1, GWTP1	SW1, GW1	100
PipeF-SW1/GW1	SWTP1, GWTP1	SW1, GW1	100
PipeG-SW2/GW2	SWTP2, GWTP2	SW2, GW2	80

a All the pipe sections were approximately 20–25 years old.

2.2. SEM–EDX

The outward view, inward view (facing the pipe wall) and the cross-section of corrosion scales were recorded by using SEM (Hitachi 7500, Japan) and the elemental composition of targeted area was measured by using EDX.

2.3. XRD

The XRD (D/max-rA, Rigaku, USA) operation parameters were: Cu Kα radiation at 40 kV and 100 mA, the 2θ ranged from 3° to 70° with a 0.02° step, and a 0.15 s count time at each step. Crystalline phase was identified using the Jade XRD software, and crystalline phase composition of the corrosion scales was quantitatively determined by contrasted parameters of intensity method (Chung, 1975).

2.4. Free and amorphous iron extractions

Since XRD can only determine the crystalline phases, the total iron, free and amorphous iron concentrations were analyzed by digestion and dithionite–citrate–bicarbonate (DCB) technique (Lin et al., 2001), respectively. Duplicate freeze-dried

samples (approximately 0.3 ± 0.0001 g) were microwave digested by using HCl, HNO_3 and HF (3:1:0.57, v:v:v) and the total iron concentration were determined by the Inductively Coupled Plasma-Optical Emission Spectrometer (ICP-OES, Perkin–Elmer Optima 2000, USA). The operation process of DCB extraction was in accordance with the method described by Tan (1996).

2.5. TOC analysis

The TOC content in scale samples was determined by TOC analyzer (Apollp 9000, Tekmar-Dohrmann, USA). Before analysis, the samples were decarbonated using 25% H_3PO_4.

2.6. Surface area and pore analysis

The TriStar II 3020 surface area and porosity analyzer (Micromeritics, Norcross, GA) was used to determine the specific surface area and pore size of powder samples by N_2 gas adsorption and desorption. The samples were degassed at 120 °C prior to analysis.

2.7. Evolutionary polynomial regression

Evolutionary polynomial regression was applied to investigate the relationship between surface area of scale sample and its iron oxide composition, and the sensitivity of the explanatory variables was analyzed. Evolutionary polynomial regression is a hybrid data-driven technique developed by Giustolisi and Savic (2006). The selection of this method was based on its incorporation of the powerful regression capability of the conventional numerical regression techniques and the superior solution searching power of genetic programming. Equations were constructed by evolutionary polynomial regression in two stages: (i) model structure search using genetic algorithm (GA); and (ii) parameter estimation by means of least square (LS) method. The equations were evaluated and selected using CoD.

$$\mathrm{CoD} = 1 - \frac{\sum_n \left(\hat{y} - y_{obs}\right)^2}{\sum_n \left(y_{obs} - \overline{y}_{obs}\right)^2} \quad (1)$$

There are several optional forms of functions and this study used the following form:

$$Y = a_0 + \sum_{j=1}^{m} a_j \cdot f\left((X_1)^{ES(j,k+1)} \cdot \ldots \cdot (X_k)^{ES(j,2k)} \right) \quad (2)$$

Where X_k is the kth explanatory variable, ES is the matrix of unknown exponents, a_j are unknown polynomial coefficients, m is the number of polynomial terms, a_0 is the bias term and f is a function selected by the user.

This technique has been applied to various fields such as pipe break prediction for water distribution systems (Xu et al., 2011), soil moisture content estimation (Elshorbagy and El-Baroudy, 2009) and so on. In this work, it was used to model the relationship between surface area of scale samples and different iron oxides content. A set of pseudo-polynomial equations were obtained by evolutionary polynomial regression, and they were selected based on the fitness to the observed data, the equation parsimony and possibility to describe the physical phenomenon, etc.

2.8. XRF

The elemental composition of corrosion product samples was determined by XRF (Advant' XP, Thermo Electron, Switzerland). The XRF spectrometer with a Lawrencium (Lr) excitation tube was employed with voltage of 0–70 kV, and with current of 0–120 mA.

3. Results and discussion

3.1. Morphology and classification of corrosion scales

Based on the visual appearance of all the harvested pipe sections, pipe corrosion scales could be divided into three categories. Category I was developed on heavily corroded pipe inner surfaces. Corrosion products exhibited typical mound-like shapes, the so-called corrosion tubercles (Fig. 1a). Corrosion tubercles either densely distributed on pipe surface or neighboring tubercles connected to each other with an appearance of a continuous thick layer (Fig. 1b). The structural features of such kind of tubercle-formed corrosion scales had been described by Sarin et al. (2001, 2004a,b). Because the top surface layer is very thin and tightly clings to hard shell layer (HSL), the samples including both the hard shell layer and the top surface layer were denoted as "THS" (top surface and hard shell). The soft and porous core layer (PCL) with high moisture content usually have four different appearances: (1) black; (2) yellow; (3) yellowish-brown; (4) black material marbled with veinlets of yellowish-brown material or yellowish-brown material marbled with black material. Some corrosion tubercles exhibit homogeneous structure and did not have distinct boundary between HSL and PCL, which was denoted as "ET" (entire tubercle). Corrosion scales of category I were mostly observed on pipes historically transporting surface waters.

Category II of the corrosion scales was relatively smooth and much thin (only few millimeters or less than a millimeter). This category of corrosion scales had no tubercles or very few tubercles sporadically distributed on inner pipe surfaces. Fig. 1c shows the typical appearance of such corrosion scales. The rather thin corrosion scale was denoted as "TNCS" (thin corrosion scale). Corrosion scales of category II were mostly observed on pipes historically transporting finished ground waters.

Category III of corrosion scales is hollow tubercles (denoted as "HT", Fig. 1d). The morphology of hollow tubercles has not been reported in previous studies on corrosion scales in DWDS. It only has a hard shell layer which was less than a millimeter thickness. The hollow tubercles might be formed by under-deposit corrosion, of which the main features were the formation of small occluded areas under-deposit. According to Brennenstuhl, microorganisms (Brennenstuhl et al., 1993), particularly sulfate reducing bacteria (SRB) and methanogenic bacteria, might play important roles in the formation process of hollow tubercles: SRB convert SO_4^{2-} to

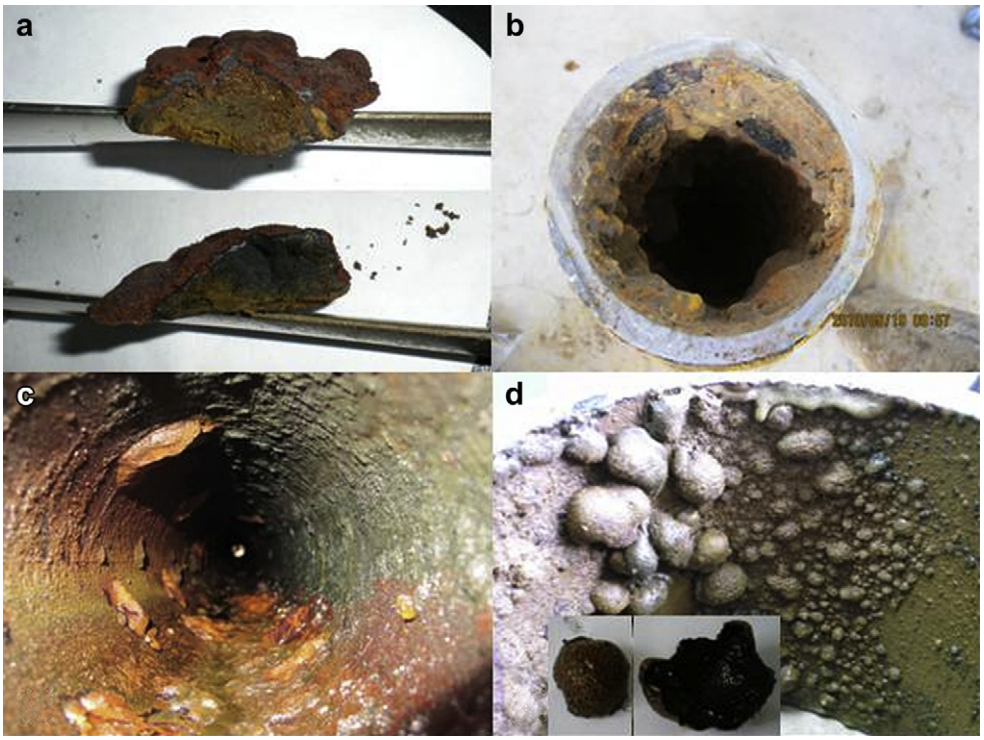

Fig. 1 – Appearance of corrosion scales on cast iron pipe internal surfaces. (a) Tubercles, (b) Pipe-SW2, (c) PipeC-GW3, (d) hollow tubercles on PipeB-GW3.

H_2S, and methanogenic bacteria drive calcite deposition which envelopes the tube area thus creating stable crevices under which corrosion takes place. Corrosion scales of category III were only observed on pipes historically transporting finished ground waters.

Compared with the surface water (SW) sources, the groundwater (GW) sources had higher alkalinity, higher hardness and relatively lower disinfectant concentration (Table 1). Except for the finished water of GWTP2, the chloride, sulfate concentrations and Larson ratio (LR) of surface waters (SW 1–3) were higher than those of ground waters (GW 1 and GW 3). LR had been used to evaluate the corrosiveness of water against iron-based pipes, which was developed based on the relative corrosive behaviors of chloride plus sulfate and the protective properties of bicarbonate for iron pipe corrosion. LR value above 0.5 was considered corrosive (Larson and Skold, 1958).

In addition, the dissolved oxygen (DO) of finished GW was generally lower than those of finished SW (data not show in Table 1). Higher chlorine and DO tend to increase the corrosion rate, while higher hardness and alkalinity can reduce water corrosivity (McNeill and Edwards, 2001; Schock and Lytle, 1999). The water quality discrepancy of SW and GW might be responsible for their corrosion scale morphology differences; the more corrosive SW could facilitate the formation of thick corrosion scales or densely distributed tubercles. The higher seasonal temperature variations of surface waters might also play some roles in the formation of heavier corrosion scales. The water temperature ranges and average values of all finished waters are provided in Table 1.

3.2. *SEM–EDX analysis of the corrosion scales*

To reveal the microstructure of the pipe corrosion scales, some typical SEM images are shown in Fig. 2. The layered structure of corrosion tubercles (Category I) can be clearly observed from the cross section of SEM images (Fig. 2a and b): top surface layer, HSL, and PCL underneath HSL. The thickness of the HSL was about several hundred microns. According to Świetlik et al. (2012) the tubercles' shell thickness may be dependent on the age and size of corrosion tubercles as well as on the quality of contact water and corrosion products composition. However, for the TNCS scales (Category II) and the HT scales (Category III), layered structure could not be observed (Fig. 2c and d). Fig. 2e–h showed the magnified images of core layer in Fig. 2a and b, part of Fig. 2c and the cluster-shaped area in Fig. 2d, respectively. EDX analysis combined with XRD results (shown in the following section) indicated that the minerals in Fig. 2e were green rust (flower-shaped minerals) and magnetite (cube type crystals), while minerals in Fig. 2f were mainly composed of magnetite (spherical mineral), goethite (acicular mineral) and akaganeite (hexagon mineral). The leaf-shaped materials in Fig. 2c and h were goethite or lepidocrocite, however the magnified image of part of Fig. 2c shown in Fig. 2g was magnetite (stacked polyhedron minerals) (Cornell and Schwertmann, 2003).

3.3. *XRD analysis of corrosion scales*

Of the pipe sections excavated from 12 DWDS sites, totally up to 69 corrosion scale samples were collected for XRD analysis,

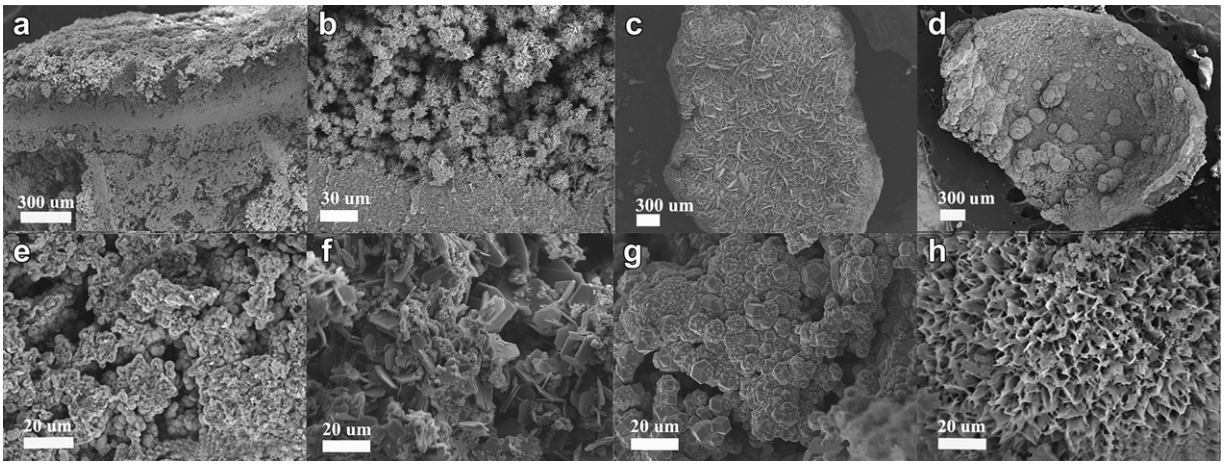

Fig. 2 – SEM images of iron pipe corrosion scales. (a) Pipe-SW3 scale cross section (×60), (b) PipeC-SW1/GW1 scale cross section (×500), (c) PipeB-GW3 thin corrosion scale ("TNCS") inside view (×35), (d) PipeB-GW3 hollow tubercle ("HT") inside view (×35), (e) and (f) were the magnified images of the PCL of (a) and (b), respectively (×1000), (g) and (h) were the magnified images of a part of (c) and cluster-shaped mineral in (d) (×1000).

and the samples included corrosion products of different apparent features. For 58 of the 69 samples, magnetite (Fe_3O_4) and goethite (α-FeOOH) were the main crystalline iron minerals, and the content of magnetite plus goethite averaged 70% (Fig. S1, supporting information). Other iron oxides contents, such as, lepidocrocite (γ-FeOOH), siderite ($FeCO_3$), green rust ($Fe_6(OH)_{12}CO_3$), hematite (Fe_2O_3), akaganeite (β-FeOOH), iron carbonate hydroxide hydrate ($Fe_6(OH)_{12}CO_3 \cdot 2H_2O$), honessite ($Ni_6Fe_2^{+3}(SO_4)(OH)_{16} \cdot 4H_2O$) and pyrite ($FeS_2$) varied significantly with water source histories or hydraulic conditions. For 9 of 69 samples, non iron corrosion minerals were found to have relatively high content (Fig. S1), such as quartz (SiO_2), calcite ($CaCO_3$), albite ((Na,Ca)$Al(Si,Al)_3O_8$), microcline ($K(AlSi_3)O_8$), gypsum ($CaSO_4 \cdot 2H_2O$) and so on. Only 2 of 69 samples, Pipe-SW3-THS scale and Pipe-SW3-PCL scale contained a large amount of $Fe_6(OH)_{12}CO_3$ and $Ni_6Fe_2^{+3}(SO_4)(OH)_{16} \cdot 4H_2O$, while the total amount of Fe_3O_4 and α-FeOOH only accounted for 15% and 4% in these two samples. Six XRD patterns of representative scale samples were provided in Fig. S2.

Green rusts are hydrated ferrous-ferric compounds having Cl^-, SO_4^{2-}, or CO_3^{2-} anions as part of their composition and were reported by many researchers as the corrosion products of iron, low carbon and stainless steels (Benjamin et al., 1996; Nawrocki et al., 2010; Świetlik et al., 2012; Tuovinen et al., 1980). Only GR1-CO_3 was discovered as the iron corrosion product in this work.

A recent study reported that pretreatment process could influence the original crystalline composition of iron corrosion products (Świetlik et al., 2012). Results of XRD, surface area and porosity analysis of corrosion scale samples pretreated under anaerobic and aerobic conditions were compared (Table 3). For scales of PipeF-SW1, GW1-ET, aerobic milling followed by vacuum-freeze-drying decreased the content of Fe_3O_4 and β-FeOOH, while increased the content of α-FeOOH and $FeCO_3$. For the same scales, aerobic milling followed by air-drying decreased β-FeOOH content, and increased α-FeOOH and γ-FeOOH content. As for scale of PipeC-GW3-ET, $FeCO_3$ increased and Fe_3O_4 decreased slightly after aerobic milling followed by vacuum-freeze-drying. Such

Table 3 – The influence of sample pretreatment on the corrosion products composition (%), surface area (m^2/g), pore volume (mL/g) and pore diameter (nm).

Sample ID	α-FeOOH	Fe_3O_4	γ-FeOOH	$FeCO_3$	β-FeOOH	$CaCO_3$	SiO_2	BET surface area	BJH desorption surface area	BJH pore volume	BJH average pore diameter
PipeF-SW1/GW1 ET-1[a]	34	43	4	0	19	0	0	53.7	36.9	0.08	9.1
PipeF-SW1/GW1 ET-2[b]	43	36	3	6	12	0	0	48.3	36.5	0.08	8.9
PipeF-SW1/GW1 ET-3[c]	50	45	5	0	0	0	0	51.4	35.2	0.07	8.2
PipeC-GW3 ET-1[a]	11	54	0	11	0	18	6	39.0	32.3	0.07	9.0
PipeC-GW3 ET-2[b]	10	48	0	14	0	18	10	53.8	44.7	0.09	8.0
PipeC-GW3 ET-3[c]	14	55	0	9	0	6	16	81.3	66.5	0.11	6.4

a milling in anaerobic glove box followed by vacuum-freeze-drying.
b milling in air followed by vacuum-freeze-drying.
c milling in air followed by air-drying.

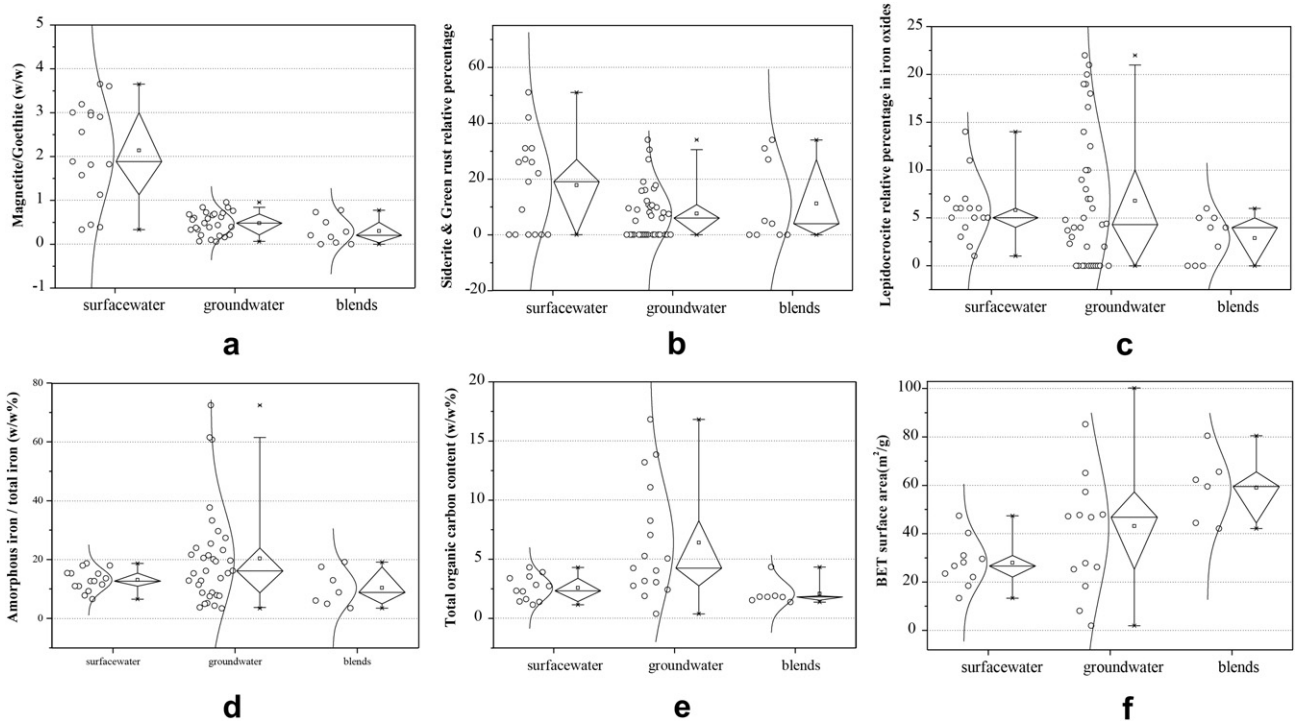

Fig. 3 – Composition characteristics of iron pipe corrosion scales with different source water histories.

changes indicated that aerobic milling could convert Fe_3O_4 into $FeCO_3$ as a result of the CO_2 exposure. After aerobic milling followed by air-drying, the scale of PipeC-GW3-ET had decreased $FeCO_3$ content and increased α-FeOOH content. Aerobic drying was found to convert the unstable β-FeOOH and Fe(II) into more stable phases such as α-FeOOH. Due to the chemical composition changes, the surface area and porosity of samples under different storage environment and drying method could also change significantly. Thus, characterization of the corrosion scales should be conducted with great caution to protect the transformation of constituents.

3.4. *Statistical analysis for scale chemical composition*

63 corrosion scale samples from different pipe segments with different source water histories were collected and the statistic box plots for their chemical composition are presented in Fig. 3. Excluding non iron minerals, different iron oxides percentages in all iron minerals were analyzed statistically. The mean value of Fe_3O_4 to α-FeOOH mass ratios (M/G) of scales receiving SW was 2.1, while the mean M/G ratios of scales receiving GW and blends were 0.5 and 0.3, respectively (Fig. 3a). However, the mean M/G ratio of 8 HT scales which only existed in pipes transporting GW was 2.5. According to Cornell and Schwertmann (2003) magnetite which contain a great deal of Fe(II) has much higher electronic conductivity than other iron oxides, thus the magnetite presented in shell-like layer and porous core favors electrons movement. Compared with scales of GW pipes, corrosion scales of SW pipes had integrated, hard shell layer and thick scales, which had much higher percentage of ferrous iron oxides such as Fe_3O_4, $Fe(OH)_2$, $FeCO_3$ etc. Besides, average $FeCO_3$ and $Fe_6(OH)_{12}CO_3$ contents (as corrosion intermediate products) of scales receiving SW were much higher than those of scales receiving GW. The relatively higher Fe_3O_4, $FeCO_3$ and $Fe_6(OH)_{12}CO_3$ content and much thicker scales on SW pipes indicated that the SW pipes were in a relatively more active corrosion status than the GW pipes. The average γ-FeOOH content of scales receiving GW was much higher than that of scales receiving SW and blends. Mean ratios of amorphous

Table 4 – Equations obtained by evolutionary polynomial regression.*

EPR equations	CoD
(a) $BET = 2475.9S^2 - 59.5M^{0.5} + 61.0$	0.39
(b) $BET = 2626.2S^2 + 72.6GR^{0.5} - 60.9M^{0.5} + 47.5G^{0.5} + 24.5$	0.65
(c) $BET = 2458.8S^2 - 121.4M^{0.5} + 368.9G \times GR^{0.5} + 916.0G \times M^2 + 66.8$	0.72
(d) $BET = 2568.7S^2 - 129.9M^{0.5} + 230.0M^{0.5} \times A + 1349.7G \times GR^{0.5} \times Am^{0.5} + 1164.5G \times M^2 + 64.0$	0.83

* BET – surface area by BET method; S – siderite; GR – green rust; M – magnetite; G – goethite; A – akaganeite; Am – amorphous iron oxide.

iron oxides to total iron oxides of GW pipe scales were also higher than those of SW pipe scales. The average TOC content of scales receiving GW was 6.4%, significantly higher than that of scales receiving SW. However, the TOC concentration of finished SW (in the range of 1–2 mg/L, data are not given in Table 1) were usually a little higher than that of finished GW. This phenomenon might be attributed to the absorbability difference of different corrosion scales. Mean values and median percentiles of BET surface area for pipe scale samples receiving GW and blends were much higher than those of samples receiving SW. Thus, the scales of GW pipes could have relatively higher sorption capacity for organic matter and other impurity because they had larger amount of amorphous iron oxides (with higher surface area) and no compact shell layer protection. Unstable iron oxide β-FeOOH was primarily present in pipes receiving GW and blends (Fig. S3).

To summarize briefly, except for HT scales on pipes receiving GW, the M/G ratios of scales on GW pipes were less than 1, but M/G ratios of scales on SW pipes were mostly more than 1. The M/G ratio could be used as a criterion of identifying corrosion scales formed under different water conditions. The pipes receiving SW were in a relatively more active corrosion status indicated by the relatively higher ferrous content (such as $FeCO_3$ and $Fe_6(OH)_{12}CO_3$) and the thickness of their corrosion scales. Relatively higher content of unstable ferric components (such as γ-FeOOH, β-FeOOH and amorphous iron oxides) existed in scales of pipes receiving GW which was less corroded. Most of the BET surface areas of scales on GW and blends pipes were larger and thus might have higher sorption capacity.

3.5. *Surface area and pore analysis*

As the corrosion scales were primarily constituted of iron oxides, the relationships between scale surface area and its iron oxides content (goethite, magnetite, green rust, siderite, akaganeite, lepidocrocite and amorphous iron oxide) were investigated by Pearson correlate analysis using SPSS 18. The correlation coefficient of each iron oxide with surface area was in the range of −0.36 to 0.30, and the R^2 of multiple linear regression equation of iron oxides contents with surface area was only 0.47. Because no empirical formula could be used for reference, the data-driven technique evolutionary polynomial regression was chosen to find if nonlinear relationship exist between the variables. The iron oxides contents of 30 corrosion scale samples used as evolutionary polynomial regression input data are plotted in Fig. S4. Five equations were selected according to their selected explanatory variable numbers (Table 4). The fitness of equations to observed data improved rapidly when new explanatory variables were introduced (seen in Fig. S5a). In order to better understand the variation of surface area in response to changed relevant input variables, the sensitivity analysis was conducted with a disturbance of the inputs by mean ± 2 STDEV (Fig. S5b) and evolutionary polynomial regression eq. (b) was selected as the best model of the relationship. To illustrate the different ranges of different input variables in a single plot, all the ranges were linearly mapped to a range of 0–100%. When one variable varied, the others changed according to the ratio of

Table 5 – Statistical summary of trace element contents in pipe scale samples (μg/g).

Element	Average	Standard deviation	Minimum	10th percentile	Median	90th percentile	Maximum	Element	Average	Standard deviation	Minimum	10th percentile	Median	90th percentile	Maximum
Mn	1008	542	144	383	1040	1525	3100	V	42	39	8	15	28	87	182
Br	344	1102	0	0	0	424	5870	Cr	42	64	0	0	18	110	281
Zn	234	286	0	18	97	544	1560	La	25	27	0	0	30	60	93
Ti	226	394	0	16	65	490	1800	Pb	15	38	0	0	0	49	216
Mo	71	41	0	0	72	129	156	W	14	27	0	0	0	64	83
Ba	70	122	0	0	0	247	460	Pt	12	35	0	0	0	29	184
Ni	60	43	0	0	68	114	134	Au	9	27	0	0	0	23	133
Cu	56	81	0	0	18	175	328	As	6	16	0	0	0	34	68
Sr	55	69	0	0	25	148	309	Rb	4	13	0	0	0	11	68
Ta	54	56	0	0	52	148	184	Bi	3	8	0	0	8	0	30

their mean values with a constraint that the sum of all the variables was equal to 100%.

Fig. S5b shows that the sensitivity of BET surface area is high to goethite and magnetite which were the dominant components (Fig. S4), but the changing trends were opposite for the goethite and magnetite. According to Cornell and Schwertmann (2003), the BET surface area of natural goethite, magnetite, green rust and siderite were 8–200 m^2/g, 4–100 m^2/g, 33.3–47 m^2/g, 7.1–38.3 m^2/g, respectively. The scale samples with M/G ratios less than 1 were mostly discovered on pipes transporting GW and blends, and the samples with higher surface area also were mostly found on pipes transporting GW (seen in Fig. 3f). The corrosion scales of pipes receiving GW mostly had higher BET surface area owing to its low magnetite content, and therefore it might have high adsorption capacity. Based on the average pore diameter data of corrosion scale samples (Table S1), the microstructure of scales from GW pipes was more porous than that of other scales.

3.6. *Elemental composition analysis by XRF*

Table 5 summarizes the average concentrations, standard deviations, maximum and minimum concentrations and selected percentiles of non-iron elements in 58 corrosion scale samples. As aforementioned, the dominant element in the 58 scale samples was iron, with mean percentage of 51%. Other non-iron elements could be classified into 3 levels: Level I (accounted for 2.45–0.1%) included in the order of

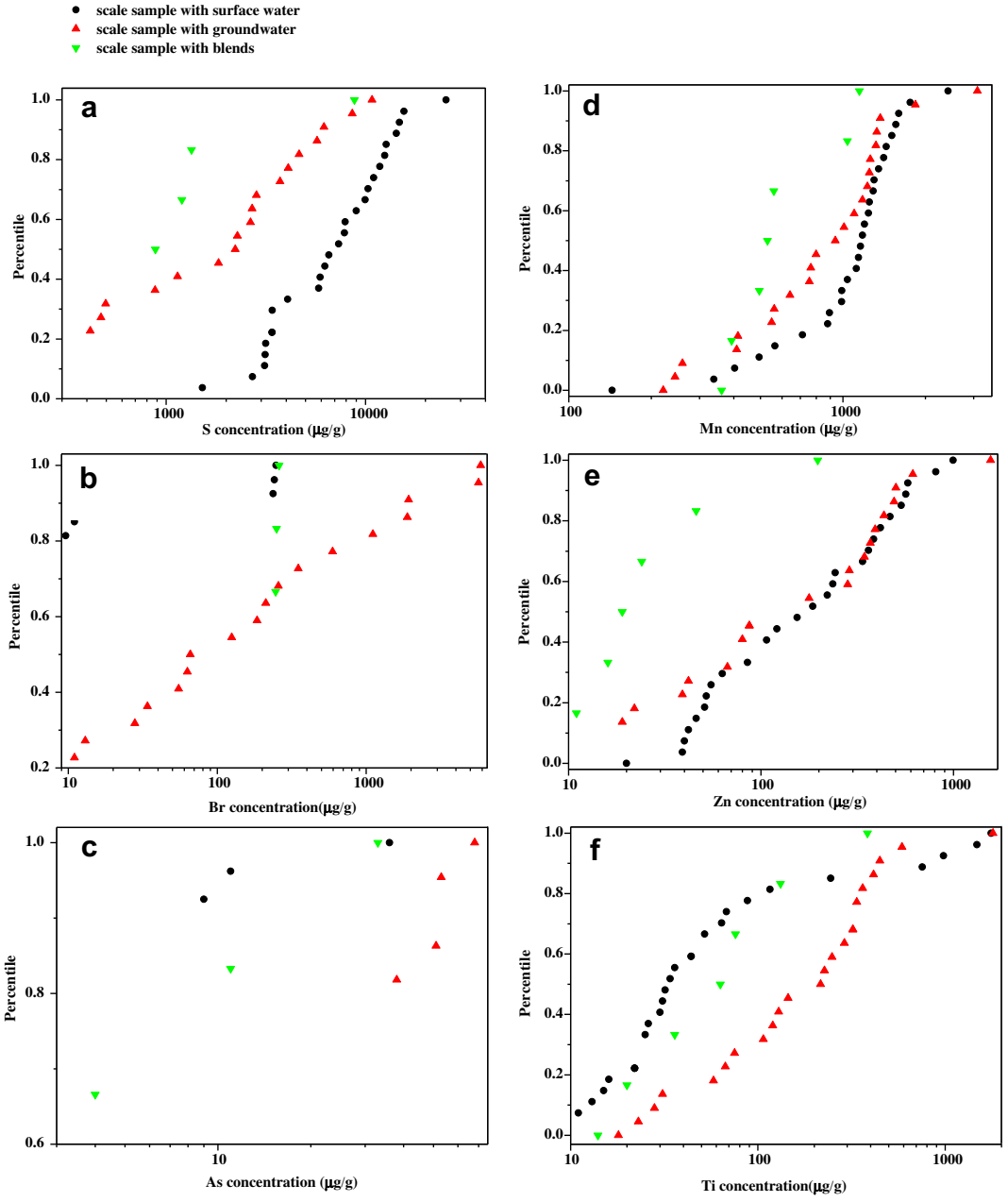

Fig. 4 – Cumulative occurrence profiles for S (a), Br (b), As (c), Mn (d), Zn (e) and Ti (f) of iron pipe corrosion scales with different source water history.

decreasing abundance: Si, Ca Al, S, Cl, Mg, K, Px, Na and Mn; Level II (0.034–0.0025%) included Br, Zn, Ti, Mo, Ba, Ni, Cu, Sr, Ta, V, Cr, and La; Level III (0.0015–0.00026%) included Pb, W, Pt, Au, As, Rb, and Bi. Less than 7 samples detected trace level of Y, Ar, Ga, U, Re, Ir, Th, Hf, Ge, Nb, Tl, Sc, Cs, Se, In or Pu. Peng et al. investigated 46 iron corrosion product samples provided by 20 drinking water utilities in United States and gave a detailed report about the common major elements and major inorganic contaminants in solid samples (Peng et al., 2010, 2012). The findings in this work were based on pipe scale samples collected from Beijing DWDS and exhibited many differences from Peng's work. The main trace inorganic elements in this study were Br and heavy metals (Table 5). Fig. 4 shows the cumulative major trace elements occurrence profiles for pipe samples with different water source histories. The profiles of Zn and Mn above 60th percentile for pipes receiving SW and GW were similar, while the contents of Mn for pipes receiving SW were higher below the 60th percentile (Fig. 4d). The profiles of S, Br, As and Ti for pipes with different water source history were significantly dissimilar. The concentrations of sulfur for pipes receiving SW were higher across the entire range. Br, Ti, Ba, Cu, Sr, V, Cr, La, Pb and As had higher levels in corrosion scales of pipes transporting GW (Fig. 4 and Fig. S6). According to Peng et al., As, V, U released from mineral deposits dissolution tend to be more prevalent in groundwater because these elements are relatively more abundant in ground waters and they cannot be efficiently removed by traditional groundwater treatment plants (Peng et al., 2012).

Some elements concentrations in scale samples were well correlated (Table S2). Therefore, some metal ions discovered in pipe scale samples might be originated from pipe materials and their joints in DWDS which might contain lead, copper, cadmium, chromium and other impurities (Peng et al., 2012).

3.7. *Raman spectroscopy*

Representative Raman spectrum of corrosion scales from different water sources are presented in Fig. S7 (instrumental and operational information were also given in supporting information). The band 744 cm^{-1} revealed the existence of significant amounts of $FeCO_3$ (Tang et al., 2006). The α-FeOOH, β-FeOOH, γ-FeOOH, $Fe_8O_8(OH)_x(SO_4)_y$, α-Fe_2O_3, Fe_3O_4, γ-Fe_2O_3 and green rust were identified at the bands of 300/481/549 cm^{-1}, 380/549/722 cm^{-1}, 638 cm^{-1}, 580/715 cm^{-1}, 411/497 cm^{-1}, 532/667 cm^{-1}, 670/718 cm^{-1} and 420/510 cm^{-1}, respectively (Cornell and Schwertmann, 2003). Because the corrosion scale on pipes is the mixture of various iron oxides and minerals, the bands detected in scale samples of a specific iron oxide have a little deviation from the representative bands of the pure material. The bands 1066 and 1364 cm^{-1} were C–O stretching of CO_3^{2-} and HCO_3^-, respectively (Teng et al., 2010).

4. Conclusions

The microstructure and chemical compositions of corrosion scales with different source water histories in DWDS were characterized using SEM–EDX, XRD, free and amorphous iron extraction, TOC analysis, surface area and pore analysis, XRF and Raman spectroscopy. Due to the water quality characteristics and corrosiveness discrepancies of different water sources, the densely distributed tubercles and thick continuous scales, which were formed as the connection of growing tubercles, were mostly found in pipes transporting surface water, but the thin (only few millimeters or less than a millimeter thick) scales and hollow tubercles caused by under-deposit corrosion were mostly discovered in pipes transporting groundwater. The SEM–EDX images exhibited the classical multilayered structure of tubercles, hollow tubercles and iron oxide minerals with various shapes. XRD results showed that magnetite (Fe_3O_4) and goethite (α-FeOOH) were the main constituents of crystalline iron minerals. Lepidocrocite (γ-FeOOH), siderite ($FeCO_3$), green rust ($Fe_6(OH)_{12}CO_3$), akaganeite (β-FeOOH), honessite ($Ni_6Fe_2^{+3}(SO_4)(OH)_{16}\cdot 4H_2O$) and other iron oxides varied significantly with source water qualities. Different pretreatment conditions had great influence on microstructure and chemical composition of corrosion scale samples.

The statistical analysis of corrosion scales with different source water histories revealed that (1) the tubercles and thick scales on surface water pipes and the hollow tubercle shells on groundwater pipes had higher M/G ratio (greater than 1.0), while the thin scales on groundwater pipes had no magnetite or with much lower M/G ratio (less than 1.0). The M/G ratio might be an important indicator for corrosion scale identification. According to the analysis of surface area and iron oxide composition, corrosion scales on groundwater pipes with lower magnetite content had larger surface area and possibly higher sorption capacity. (2) Compared with the pipes transporting ground water, the pipes transporting surface water were more seriously corroded and in relatively more active corrosion status, indicated by their higher siderite, green rust and total iron contents. (3) Higher content of unstable ferric components such as γ-FeOOH, β-FeOOH and amorphous iron oxide existed in scales of pipes receiving groundwater which was less corroded. (4) The primary trace inorganic elements in scale samples were Br and heavy metals; and Br, Ti, Ba, Cu, Sr, V, Cr, La, Pb and As had higher levels in scale samples of pipes transporting groundwater.

The characterization and classification of distinct corrosion scales developed under different water conditions could help to understand the red water mechanisms triggered by source water switch.

Acknowledgment

This work was supported by National Natural Science Foundation of China (No. 51178450 and No. 51025830) and Water Pollution Controls and Treatment Technologies Special Project of China (2009ZX07424-003).

Appendix A. Supplementary data

Supplementary material associated with this article can be found, in the online version, at http://dx.doi.org/10.1016/j.watres.2012.07.031.

REFERENCES

American Water Works Association Research Foundation and DVGW-Technologiezentrum Wasser, 1996. Internal Corrosion of Water Distribution Systems, second ed. American Water Works Association, Denver, CO.

AWWA, 1999. AWWA Report: $325 Billion for Pipes, AWWA Mainstream, p. 3 (Feb.).

Benjamin, M.M., Sontheimer, H., Leroy, P., 1996. Corrosion of iron and steel. Cooperative Research Report. In: Internal Corrosion of Water Distribution Systems. AWWA Research Foundation, Denver, CO, pp. 29–70.

Brennenstuhl, A.M., Gendron, T.S., Cleland, R., 1993. Mechanisms of underdeposit corrosion in freshwater cooled austenitic alloy heat exchangers. Corrosion Science 35 (1–4), 699–711.

Brodeur, T., Davis, F.S., Florence, R., Kim, M., Craig, M., Gianatasio, J., Sharp, D., Lowe, P., 2006. From red water to pump failures-corrosion control activities & related studies. Florida Water Resources Journal (12), 42–48.

Chung, F.H., 1975. Quantitative interpretation of X-ray diffraction patterns of mixtures. III. Simultaneous determination of a set of reference intensities. Journal of Applied Crystallography 8 (1), 17–19.

Cornell, R.M., Schwertmann, U., 2003. The Iron Oxides: Structure, Properties, Reactions, Occurrence and Uses. Wiley-VCH Verlag GmbH & Co. KGaA, Weinheim, 703 pp.

Elshorbagy, A., El-Baroudy, I., 2009. Investigating the capabilities of evolutionary data-driven techniques using the challenging estimation of soil moisture content. Journal of Hydroinformatics 11 (3–4), 237–251.

Gerke, T.L., Maynard, J.B., Schock, M.R., Lytle, D.L., 2008. Physiochemical characterization of five iron tubercles from a single drinking water distribution system: possible new insights on their formation and growth. Corrosion Science 50 (7), 2030–2039.

Giustolisi, O., Savic, D.A., 2006. A symbolic data-driven technique based on evolutionary polynomial regression. Journal of Hydroinformatics 8 (3), 207–222.

Larson, T.E., Skold, R.V., 1958. Laboratory studies relating mineral quality of water to corrosion of steel and cast iron. Journal of AWWA 14 (6), 285–588.

Lin, J.P., Ellaway, M., Adrien, R., 2001. Study of corrosion material accumulated on the inner wall of steel water pipe. Corrosion Science 43 (11), 2065–2081.

McNeill, L.S., Edwards, M., 2001. Iron pipe corrosion in distribution systems. Journal American Water Works Association 93 (7), 88–100.

Nawrocki, J., Raczyk-Stanisławiak, U., Świetlik, J., Olejnik, A., Sroka, M.J., 2010. Corrosion in a distribution system: steady water and its composition. Water Research 44 (6), 1863–1872.

Peng, C.Y., Korshin, G.V., Valentine, R.L., Hill, A.S., Friedman, M.J., Reiber, S.H., 2010. Characterization of elemental and structural composition of corrosion scales and deposits formed in drinking water distribution systems. Water Research 44 (15), 4570–4580.

Peng, C.Y., Hill, A.S., Friedman, M.J., Valentine, R.L., Larson, G.S., Romero, A.M.Y., Reiber, S.H., Korshin, G.V., 2012. Occurrence of trace inorganic contaminants in drinking water distribution systems. Journal American Water Works Association 104 (3), 181–193.

Ray, R.I., Lee, J.S., Little, B.J., Gerke, T.L., 2010. The anatomy of tubercles: a corrosion study in a fresh water estuary. Materials and Corrosion 61 (12), 993–999.

Reiber, S., Poulsom, S., Perry, S.A.L., Edwards, M., Patel, S., Dodrill, D.M., 1997. A General Framework for Corrosion Control Based on Utility Experience. American Water Works Association, Denver, CO, 326 pp.

Sarin, P., Snoeyink, V.L., Bebee, J., Kriven, W.M., Clement, J.A., 2001. Physico-chemical characteristics of corrosion scales in old iron pipes. Water Research 35 (12), 2961–2969.

Sarin, P., Snoeyink, V.L., Bebee, J., Jim, K.K., Beckett, M.A., Kriven, W.M., Clement, J.A., 2004a. Iron release from corroded iron pipes in drinking water distribution systems: effect of dissolved oxygen. Water Research 38 (5), 1259–1269.

Sarin, P., Snoeyink, V.L., Lytle, D.A., Kriven, W.M., 2004b. Iron corrosion scales: model for scale growth, iron release, and colored water formation. Journal of Environmental Engineering 130 (4), 364–373.

Schock, M.R., Lytle, D.A., 1999. Internal corrosion and deposition control. Chapter 17. In: AWWA, Edzwald, J.K. (Eds.), Water Quality and Treatment: a Handbook of Community Water Supplies, fifth ed. J.K. McGraw-Hill Companies, New York, NY.

Tan, K.H., 1996. Soil Sampling, Preparation, and Analysis. CRC Press, Marcel Dekker, New York.

Tang, Z.J., Hong, S.K., Xiao, W.Z., Taylor, J., 2006. Characteristics of iron corrosion scales established under blending of ground, surface, and saline waters and their impacts on iron release in the pipe distribution system. Corrosion Science 48 (2), 322–342.

Teng, D., Zheng, L., Zhu, C.G., 2010. Investigation of seawater-anions aqueous solutions by Laser Raman spectrometry. Laser Journal (in Chinese) 31 (4), 21–23.

Tuovinen, O.H., Hsu, J.C., 1982. Aerobic and anaerobic microorganisms in tubercles of the Columbus, Ohio, water distribution system. Applied and Environmental Microbiology 44 (3), 761–764.

Tuovinen, O.H., Button, K.S., Vuorinen, A., Carlson, L., Mair, D.M., Yut, L.A., 1980. Bacterial, chemical, and mineralogical characteristics of tubercles in distribution pipelines. Journal American Water Works Association 72 (11), 626–635.

Wang, L.P., 2007. Study of Iron Stability Problem and Pipes Corrosion in Drinking Water Distribution System. Master Dissertation, Tianjin University.

Xu, Q., Chen, Q.W., Li, W.F., Ma, J.F., 2011. Pipe break prediction based on evolutionary data-driven methods with brief recorded data. Reliability Engineering and System Safety 96 (8), 942–948.

Świetlik, J., Raczyk-Stanisławiak, U., Piszora, P., Nawrocki, J., 2012. Corrosion in drinking water pipes: the importance of green rusts. Water Research 46 (1), 1–10.